NACA TM 1271

NATIONAL ADVISORY COMMITTEE FOR AERONAUTICS

TECHNICAL MEMORANDUM 1271

EFFECT OF INTENSE SOUND WAVES ON A STATIONARY GAS FLAME

By H. Hahnemann and L. Ehret

Translation of "Über den Einfluss starker Schallwellen auf eine Gasflamme." Zeitschrift für Technische Physik Nr. 10-12, 1943

Washington
July 1950

NATIONAL ADVISORY COMMITTEE FOR AERONAUTICS

TECHNICAL MEMORANDUM 1271

EFFECT OF INTENSE SOUND WAVES ON A STATIONARY GAS FLAME*

By H. Hahnemann and L. Ehret

SUMMARY

With the help of a new kind of sound generator, intense sound vibrations were imparted to a stationary propane-air flame issuing from a nozzle. In addition to a slight increase of the flame velocity, a fundamental change both in the shape of the burning zone and in the flow pattern could be observed. This was explained as a transition at the nozzle from jet flow to potential flow.

I. INTRODUCTION

The cylinder charge of an otto cycle engine burns while the gas-air mixture is in strongly turbulent motion. This turbulence, produced by the suction process, increases the burning velocity considerably and makes the operation of high-speed engines possible. When the engine knocks, there appear, in addition, pronounced local pressure differences in the cylinder. These produce sound waves of great amplitude which are reflected many times by the walls and reverberate through the mixture. As these waves also affect the combustion cycle, whether produced directly by the periodic pressure changes or indirectly by the turbulence due to reflection, the following investigations on the effect of sound waves on burning gas flames were carried out.

The sensitivity of gas flames for weak sound waves is a well-known phenomenon. R. König (reference 1) has used this property in the flame capsule named after him for the indication of sound waves, and it is still being used as a sound indicator, especially in demonstrations.

In all these cases, the flame responds to changes in speed of the gas stream caused by the weak sound waves so that Zickendraht (reference 2)

---

*"Über den Einfluss starker Schallwellen auf eine Gasflamme." Zeitschrift für Technische Physik Nr. 10-12, 1943, pp. 228-242.

denotes it directly as a speed receiver in the acoustic sense. Moreover, at sounds of high intensity, the reflections from solid walls introduce additional motions in the gas which have an effect on the combustion similar to the turbulent fluctuations (here designated as natural turbulence) produced at supercritical Reynolds numbers in the flow by amplification of the inevitable disturbances contained in the boundary layers. The effect of the natural turbulence on stationary gas flame was first investigated in detail by Damköhler (reference 3).

According to this, the turbulence changes the shape of the flame (the sharply defined bell-shaped burning surface over the burner pipe in laminar flow changes into a diffuse "bolt-shaped" form) and increases the flame speed considerably. H. Mache (reference 4) later investigated the behavior of a stationary flame burning over a vertical pipe in the transitional zone between laminar and turbulent flow.

A simple case, thoroughly investigated experimentally and theoretically, is the stationary gas flame burning from a cooled nozzle. It already had been repeatedly suggested, for instance, by A. N. J. van de Poll and Westerdijk (reference 5) and H. Mache and A. Hebra (reference 6), that the simple burner tube be replaced by a nozzle for accurate measurements. On a nozzle, the constant velocity profile over practically the whole throat insures clean and simple hydrodynamic conditions. Also the cooling of the nozzle should prevent disturbed boundary conditions caused by preheating of the gas flow. When such a nozzle is supplied with a clean flow from the mixture container, a well-defined, laminar flame cone naturally develops above it.

Because of these conditions, the nozzle burner flame appears well suitable, also, for investigating the effects of intense sounds on the flame. The following discussion represents a first contribution in this direction.

II. TEST APPARATUS AND PROCEDURE

The investigation was carried out with mixtures of commerical propane and compressed air. The experimental setup consisted of five main parts. The gas and air consumption and the composition of the mixture were determined with gas meters on the principle of flow capillaries. With the device termed "Flame Chamber," a quietly burning, well-defined nozzle flame was produced, to which could be conveyed the intense sound from a sound generator. The frequency of this sound was read on a frequency meter. The sound amplitude was measured at the sound source with a special amplitude meter. The sound intensity at the source was thus defined by the frequency and amplitude.

1. Production of Mixture and Quantitative Measurements

The setup for producing the mixture and measuring the consumption is represented diagrammatically in figure 1. The compressed air and the propane were taken from commercial gas bottles a and b. The volume of compressed air was regulated roughly with a reducing valve c and then finely adjusted with a Hofer angle valve d of 2-millimeter maximum inside width. For the fine adjustment of the propane volume, a Hofer angle valve e of 2-millimeter opening was attached direct to the propane bottle. From these needle valves d and e, the gases passed over the steadying flasks f of 3-liter content to the flow manometers h, before which, at the U tubes g, the static high pressure relative to the free atmosphere was read in millimeters water column pressure. Since, according to preliminary tests, the gas in the steadying flasks f practically assumes room temperature, no special measurements of the gas temperature were necessary. The pressure gages h for measuring the flow volume consisted of one capillary each. The pressure drop along the capillaries was read on U manometers in millimeters water column pressure. The capillary for the compressed air was 1.5 millimeters in diameter and 76 millimeters in length; that for propane, 0.55 millimeters in diameter and 78 millimeters in length. Each reading on the four U-tube manometers in each test was accompanied by a record of the room temperature and the barometric pressure.

It should be borne in mind when working with flow capillaries that the reading of these instruments is, under certain conditions, dependent upon the temperature as well as the pressure. Postulating laminar flow, that is, Reynolds numbers Re below 2300 $\left(\mathrm{Re} = \frac{\bar{u}d}{\nu}\right.$ with $\bar{u}$ = averaged speed, d = capillary diameter, $\nu = \frac{\eta}{\rho}$ = kinematic viscosity, η = coefficient of viscosity, $\left.\rho = \text{density}\right)$ the pressure drop Δp in a capillary of length l is according to Poiseuille's law

$$\Delta p = \frac{128}{\pi} \frac{l}{d^4} \eta V \tag{1}$$

with V denoting the gas volume in unit time at average pressure in the capillary. Since the viscosity coefficient η is practically unaffected by the pressure, the ratio $\frac{\Delta p}{V}$ therefore varies only a little with the temperature. To illustrate: for a mean room temperature of 20° C, $\frac{\Delta p}{V}$ varies, at most, by 1.4 percent when the temperature fluctuates by ±5° C. But in equation (1), it is assumed that the capillary length l is very great with respect to the entrance length l_a. When the inlet accelerations are not negligible, equation (1) can be rewritten as

$$\Delta p = \frac{128}{\pi} \frac{l}{d^4} \eta V + a\rho \frac{\bar{u}^2}{2} = \frac{8V}{\pi d^4}\left(16 l \eta + \frac{a}{\pi} \rho V\right) \qquad (2)$$

where a is a numerical factor. At constant flow volume V is then also dependent on Δp, since the density ρ appears, hence is then also somewhat dependent on the pressure.

Introducing for the inlet length the expression

$$l_a \approx 0.029\ d\ Re = 0.029 \frac{4}{\pi} \frac{\rho}{\eta} V \qquad (3)$$

the requirements

$$l \gg 2.5\ V(mm) \quad \text{and} \quad d > 4 \times 10^{-2}\ V(mm) \qquad (4)$$

follow immediately from equation (3) (V in cm^3/sec), when $\frac{\Delta p}{V}$ is to be unaffected by the pressure, as, for example, for air of 20° C and 760 mm Hg. Consequently, the indication of flow capillaries of sensible length is practically independent of the pressure, provided the rate of flow is very small (less than 10 cm^3/sec.).

The conditions are even worse when the Reynolds number in the relation

$$V = \frac{1}{4} \pi\ d\ \nu\ Re \qquad (5)$$

exceeds the critical value 2300. For in that instance

$$\Delta p = \left(\frac{0.158 \times 16}{\pi^2}\right)\left(\frac{l \rho^{3/4} \eta^{1/4}}{\bar{u}^{1/4} d^{21/4}}\right) V^2 \qquad (6)$$

even without allowance for the inlet processes and the transitional complications to full turbulence. So, if the flow volume is kept constant, no pressure relationship with the capillary indication Δp is at all possible in turbulent flow. In practice, Δp is usually specified as function of the normal volume rather than as function of the flow volume V. According to the cited equations, it cannot be represented by a uniform calibration curve.

For this reason, the pressure decreases Δp, the static high-pressure upstream from the capillaries, the room temperature, and barometric pressure were recorded for each flame test first, and then, after termination of the principal tests, the corresponding volumes per second were determined by collection in a pneumatic tank, the water of which was raised to room temperature. As it would take too much time to adjust all theoretical values of a principal test exactly and to wait for the correct barometric pressure, closely approximating values between the ideal values were simply interpolated. From each of the thus-defined flow volumes V_1 per second, the consumption of the normal volume V_n per second at 760 mm Hg and 0° C of the individual components of the corresponding principal tests was determined by the formula

$$V_n = \frac{b_o - e}{760} \frac{273}{T} V_1 \qquad (7)$$

where b_o represents the barometric pressure in mm Hg and e the saturation pressure of the water vapor in mm Hg at room temperature T in degrees K. These values V_n were used for computing the flame speed and the percent composition of the gas mixture.

The problem of ambiguity between pressure-drop reading and flow volume in capillary flow meters was purposely explored a little deeper because too little attention is paid to these things, as a rule, in gas laboratories; hence, too much accuracy is ascribed to the test data.

2. The Flame Chamber

After passing through the capillary flow meters, the compressed air and propane were combined and conveyed through a copper coil 3 meters long and 4 millimeters inside diameter to the actual combustion apparatus. The coil served as a mixer and also as an elastic connecting link for lifting the flame chamber off the support base. The whole apparatus, termed flame chamber for short, is shown in figure 2.

The mixture passed from the mixing coil through the inlet opening a into the outer cylindrical space b of the flame chamber into whose upper part an annular diaphragm c which was to make the gas flow irrotational as much as possible left an open slit of about 0.1 millimeter. The mixture reached the inner cylinder chamber f of 60-millimeter diameter and 30-centimeter height through 10 holes of 10-millimeter diameter each in the lower part of the inner cylinder d which were covered with close mesh screens e to act as insurance against flashback, and passed in the countercurrent upward toward the burner nozzle g of 10-millimeter throat diameter. The nozzle g could be raised and lowered about 3.5 centimeters with the thread h, that is, about a half wave length of the employed sound frequency, so that the sound chamber up to the nozzle tip could be tuned to acceptable acoustic conditions. The nozzle g was worked into a massive iron cylinder i with large outer area so that the heat transferred from the flame to the nozzle body could be dissipated as well as possible with minimum preheating of the mixture at the inner

nozzle walls. The mixture left the nozzle through a short hole k 4 millimeters high and 10 millimeters in diameter drilled in a cap piece. The short edge on the end of the hole prevented precipitation of water formed during combustion in the immediate vicinity of the combustion zone. In some of the exposures, this cap attachment was omitted.

A square protective box l of black lacquered sheet iron 21 centimeters wide by 50 centimeters high was placed over the flame chamber as protection against drafts. The box was fitted with two polished plate-glass windows m for observation and photography. The flame, which was frequently blown out by violent acoustic shocks, could be relit by a small movable hot wire igniter n. A glass measuring scale o situated next to the flame was included in the photograph to define the size of the flame. If necessary, the rod could be illuminated by a small shielded spotlight.

Fifteen minutes were allowed for the apparatus to come to equilibrium before each flame photograph. Preliminary experiments in which the change of the flame height after readjustment of the mixture composition was followed up with a cathetometer indicated that this waiting period was always sufficient for scavenging and filling the chamber with a new mixture.

Flame photographs were made natural size, or slightly larger, on 6.5- by 9-centimeter plates. The camera had a 1:3.5 lens with a 16.5-centimeter focal length. Agfa-contrast or blue-hard film was used and exposures were taken for 1/5 to 1/10 second.

The flame cones were enlarged 6 to 8 times with an enlarger, and the flame surface was calculated from these enlargements according to the graphical process explained in figure 3.

The axis a and the enveloping line b in a cut through the rotationally symmetrical flame zone were finely subdivided with the same unit ds. Verticals to base line AC were drawn through the dividing points of b; and parallel to AC, through the dividing points on axis a. The points of intersection of the even-numbered verticals and parallels to AC yield a new curve c. The 2π time value from the planimetered area ABC is, as is readily proved, the desired flame surface O. In conjunction with the normal volume V_n according to equation (7) - the subscripts L and P refer to the individual components, compressed air and propane - the percent contribution of propane to the normal volume of the mixture is

$$x_P = 100\frac{V_{nP}}{V_{nL} + V_{nP}}(\%) \qquad (8)$$

and the normal flame speed w_n referred to the normal volume is

$$w_n = \frac{V_{nL} + V_{nP}}{O} \tag{9}$$

The luminous zone on the negatives shows a certain thickness so that outer and inner surfaces could be distinguished. According to the investigations by Hübner and Klaükens (reference 7), the image on the negative gives only an approximate value of the true thickness of the luminous zone; however, an outer and inner flame surface O_a and O_i, corresponding to these boundaries, can be defined and, when these values are introduced in equation (9), an upper and a lower flame speed w_{na} and w_{ni} can be identified. The graphical evaluation of a photograph, according to these viewpoints, is shown in figure 4.

3. The Sound Generator

The flame chamber described in the foregoing was mounted gas tight by a flange on the frame of the sound generator, shown in figure 5, so that the bottom of the chamber opposite to the burner nozzle was formed by a diaphragm which served as a sound source. The complete sound transmitting setup was discussed in a previous report (reference 8)(called therein "Aerodynamic plate vibrator") and, therefore, its mode of operation will be described only briefly.

A jet of compressed air flows through a nozzle a with "supercritical" pressure ratio. A stationary flow is formed in this jet in which regions of supersonic and subsonic speed alternate along the jet axis. In consequence, if a pitot tube were moved along the axis, it would indicate a wave-shaped pressure profile. Now, when the compressed-air nozzle a (of 10-millimeter nozzle diameter) is set at such distance from the small cylinder b (10-mm inner diameter and 14.2 mm long in the present case) that the opening of b lies in a region of rising pitot pressure, then b acts as a resonator and the previously stationary flow becomes nonstationary. The extraordinarily severe sound oscillations discovered by J. Hartmann (reference 9) are originated in the resonator, and their frequency is governed essentially by the dimensions of the resonator. The frequency used in the present case was 5000 cycles per second.

The employed plate vibrator utilized the intense pressure fluctuations (order of magnitude of several atmospheres) at the base of the resonator, in which this base was itself replaced by a diaphragm. This diaphragm, made of "Elektron", was 1.8 millimeters thick and 60 millimeters in diameter with a resonant frequency of 5000 cycles per second. It was

fastened in the flange d and spaced 0.45 millimeters from the resonator end to allow for vibration. The flame chamber was fastened to this. The resonator fluctuations activated the diaphragm and were reflected into the flame chamber and conducted to the flame. The amplitude of the diaphragm vibrations could be varied over a wide range by changing the compressed-air pressure and the distance between the resonator and the compressed-air nozzle, but the frequency could be varied only slightly.

4. Amplitude and Frequency Measurements

A measure of the size of the sound waves arriving at the flame zone was necessary because the various effects could be dependent on the intensity. The safest, but also the most difficult, way was to take these measurements while the flame was being affected by the sound. An electrical circuit shown in figure 6 shows the answer to this problem.

The condenser C_x consists of the electrically insulated resonator holder e of the plate-vibrator, and the diaphragm grounded to the clamping frame d (see fig. 5) varies its capacitance in rhythm with the vibrations of the diaphragm. This condenser C_x is grounded through a 90-megohm resistor to the 100-volt direct-current battery E. The resistor R_1 was timed so that the charged condenser C_x with the battery disconnected could discharge only 1 percent in the vibration period of 1/5000 second.

The changes in the capacitance due to the diaphragm oscillations thus produce an alternating-current voltage on the condenser which acts over the 0.01 microfarad blocking condenser C_1 on the grid of a type AC_2 Telefunken tube I. Tube I is adjusted to the center of its characteristic curve with the grid voltage E_1, the grid leak R_2 of 10 megohms, and the plate voltage battery E_a, and so amplifies the alternating-current voltage which is carried through transformer Tr to the grid of a second Telefunken tube II of type AC_2. The second tube II is adjusted to the lower break of its characteristic curve with the grid voltage battery E_2, potentiometer R_3, and plate voltage E_a, and acts as alternating-current rectifier. The ammeter A in the plate circuit, the sensitivity of which is controlled by resistor R_4, therefore indicates the amplified alternating current voltage on the condenser C_x and hence the amplitude of the diaphragm oscillations. The filament voltage E_h for tube I and tube II was supplied by high-capacity storage batteries.

The above amplitude-measuring device is called instrument A. A second amplitude-measuring device, instrument B, which was available from previous investigations and which will be described more closely in a later publication, was used to calibrate apparatus A to absolute values. The diaphragm vibrations were measured simultaneously with both

A and B. For this purpose, apparatus B, which measured the variation in capacity between the grounded vibrating diaphragm and the electrically insulated key of a 1/100-millimeter-length dial gage by a modulation method, was mounted in the place usually occupied by the flame chamber. Instrument B, which, with nonvibrating diaphragm, was calibrated to absolute values by varying the distance between diaphragm and key, indicated the deflection of the diaphragm center toward the side of the flame chamber. According to estimated calculations, the difference of the capacity, on the one hand, between the key of the dial gage and the quiescent diaphragm and, on the other, between the key and the diaphragm deflected during the vibration, was negligibly small for equal distance between key and diaphragm. Similarly, the capacitive effect of the damping mass of the diaphragm plays no part.

Owing to this property of the calibration, the solely interesting amplitude toward the side of the flame chamber was always ascertained with instrument A even if the diaphragm vibrated asymmetrically about the equilibrium position. Incidentally, it is noted that static deflection of the diaphragm by the dynamic pressure of the compressed-air jet acting on the resonator cylinder b (figure 5) was consistently negligible with respect to the smallest test values of diaphragm amplitudes.

Besides the amplitude, the frequency was also necessary for the intensity calculations. For this purpose, the alternating-current voltage at transformer Tr (fig. 6) was conducted according to figure 7 through the bypass condenser C_2 of 0.02 microfarad toward the control grid of pentode III grounded through the leak R_5, amplified, and carried through the high-ohm resistor R_6 on an electrode of a glow-discharge lamp Gl. The central electrode of this lamp was grounded and the voltage of a buzzer calibrated to frequencies was connected to the third electrode at A_2 through the resistor R_7. When the two frequencies were the same, the lamp went out.

The grid of pentode III, to which the direct-current voltage E_3 was connected through resistor R_8, was short-circuited on the alternating current side by the block condenser C_3. The cathode was grounded through resistor R_9 and short-circuited on the alternating-current side by condenser C_4. The direct-current voltage E_4 was supplied to the anode through resistor R_{10}. The filament voltage E_h was supplied by a storage battery. All the resistors used in the described hookup were noninductive.

The procedure for making a test is explained in the light of a test record (table 1 and fig. 9).

First, instrument B was calibrated by the static method to absolute values; then instrument A was calibrated with apparatus B with diaphragm vibrating, the readings on both instruments being correlated to the same deflection f. The dashed curve $\bar{i}$ in figure 8 represents the dial gage

calibration of instrument B; and the solid curves, the corresponding calibration of instrument A for two values of test range resistor R_4 (wiring diagram of fig. 6). Following the calibration, the dial gage was replaced by the flame chamber and the gas mixture and flow velocity were adjusted to the desired values at the two flow pressure gages after the flame was ignited. The readings taken included the pressure differences Δp_L and Δp_P at the flowmeters, the static pressure Δp_{8L} and Δp_{8P} at the legs of the static pressure gage before the capillaries, the room temperature t, and the barometric pressure b_o. Notes were also made of the diaphragm through its characteristic value, identifying its dimensions, the length l of the inserted resonator cylinder, the adjusted distance b between resonator and static diaphragm, the characteristic value of the compressed air nozzle, and the tank pressure p_o. Upon completion of the heating-up period, the flame was subjected to sound vibrations and photographed, the deflections i_1 of ammeter A (fig. 6) and i_2 of the calibrated buzzer being read when the glow-discharge lamp Gl (fig. 7) went out. In most cases, the flame was photographed with and without sound.

The inner and outer flame surfaces were computed from the flame photographs, the diaphragm frequency ν read from the reading of the buzzer corresponding to the reading of i_2, the amplitude f of the diaphragm vibration determined from the corresponding calibration curve of instrument A as indicated, for example, in figure 8, with $\Delta i = i_1 - i_0$ (i_1 and i_0 = deflection of ammeter for vibrating and static diaphragm, respectively). The gas volume reduced to normal state was taken from the calibration curves of the two flow pressure gages corresponding to the particular test and subsequently under about the same conditions and the mixture composition and the outer and inner normal flame speed w_{na} and w_{ni} computed by equations (8) and (9).

The sound energy J radiated from a diaphragm of 60-millimeter diameter (Φ = 60 mm) into the gas mixture can be calculated (reference 8) as

$$J = \frac{\rho c}{2} (\omega f)^2 \frac{F}{5} = \frac{\pi^3}{10} \rho c (\nu f \Phi)^2 \qquad (10)$$

where ρ is the density of the gas mixture, c, the speed of sound in the gas, $\omega = 2\pi\nu$, the frequency, and F, the area of the diaphragm.

When it is assumed that there is no perceptible loss of sound energy between the diaphragm and the end section of the nozzle, the intensity J_o in the end section of the burner nozzle of D = 10 mm diameter is, therefore,

$$J_o = \frac{2}{5}\pi^2 \rho c (\nu f \frac{\Phi}{D})^2 \qquad (11)$$

With the approximate values $\rho = 1.25 \times 10^{-3}$ gm/cm^3 and $c = 3.4 \times 10^4$ cm/sec as well as the given values for D and Φ

$$J_o = 6.04 \times 10^{-4} (\nu f)^2 \left[\text{watt/cm}^2\right] \tag{11a}$$

where ν is in cycles per second and f in centimeters.

TABLE I

Number of exposure: 107 (no sound); 108 (with sound) compare figure 9	Barometric pressure: b_o = 764 mm Hg Room temperature: t = 21.9° C	Date: April 13, 1942, 14 hours
Photographic data:		
Plate: Agfa spectral blue-hard 6.5 × 9 cm^2		Lens: Zeiss-Tessar No. 716096
Exposure time: 1/10 sec		Shutter: 1:3.5
Rate of flow, flame surface, and flame speed:		
	Air side	Propane side
Capillary	Diameter: 1.80 mm; length: 76 mm	Diameter: 0.55 mm; length: 78 mm
Flowmeter reading:	Δp_L = 372 − 206 = 166 mm Hg	Δp_P = 383 − 188 = 195 mm Hg
Static pressure gage reading:	Δp_{sL} = 411 − 63 = 348 mm Hg	Δp_{sP} = 452 − 153 = 299 mm Hg
Volume in normal state: (by vibration)	V_{nL} = 84.1 cm^3/sec	V_{nP} = 4.6 cm^3/sec
Composition in percent:	x_L = 94.8 percent	x_P = 5.2 percent
Total volume:	V_n = 88.7 cm^3/sec	
	Without sound	With sound
Surface of burning cone: inner	O_i = 4.33 cm^2	3.08 cm^2
Surface of burning cone: outer	O_a = 4.60 cm^2	3.27 cm^2
Normal flame speed: inner	w_{ni} = 20.5 cm/sec	28.8 cm/sec
Normal flame speed: outer	w_{na} = 19.3 cm/sec	27.1 cm/sec
Acoustic data: Diaphragm: Hg 239 (No. 9 piece of 2 mm thickness of a series of electron AZ 855 with beaded edge, diameter Φ = 60 mm)		
Resonator: diameter: 10 mm; length: 12.4 mm		Resonator holder No. 2
Burner nozzle: diameter: 10 mm		Compressed air nozzle: D_3 with 10 mm diameter and sharp edge
Distance: diaphragm to resonator: b = 0.5 mm		Distance: resonator to compressed air nozzle: not read
Tank Pressure: p_o = 3.0 atu		Diaphragm frequency: ν = 4790 cps
Filament voltage E_h = 4 V and plate voltage E_a = 180 V on Amplitudemeter A		
Deflection of Amplitudemeter A at instrument (0.2 milliamperes, 10 millivolts, 50 ohms) with test range resistance R_4 = 9 ohms	Diaphragm, static: i_0 = 4.8 Sk.T Diaphragm vibrating: i_1 = 15.4 Sk.T	Δi = 10.6 Sk.T
Diaphragm deflection: f = 0.0132 cm (compare fig. 8)		Intensity: J_o = 2.42 watt/cm^2

III. RESULTS OF TESTS

1. Effect of Sound on Flame Speed

The measured flame speeds, determined as described above, are plotted against the propane concentration x_p for the inner edge in figure 10 and for the outer edge in figure 11. In these figures, the hollow circles with the solid average curves refer to the flame speeds without sound; all other signs refer to those with sound. The sound frequency varied only between $\nu = 4270$ and 4840 cycles per second, while the amplitude of vibration of the diaphragm f was varied from 0.01 mm to 0.23 mm. The apparatus could deliver still higher amplitudes (to f = 0.30 mm) which corresponds to an intensity of 12.5 watts per centimeter^2 in the burner nozzle, but at such sound intensities, the flame was immediately extinguished and could not be relit under any circumstances. Even with amplitudes between f = 0.15 millimeter and 0.23 millimeter, measurable flame pictures were obtained only with great difficulty, and only in the immediate vicinity of the propane concentration corresponding to maximum flame speed.

Figures 10 and 11 individually show the following: The maximal flame speed (referred to the inner surface) of the flame without sound appeared at a propane concentration of $x_p = 4.4$ percent, hence, a somewhat higher value than the stoichiometric proportion of $x_p = 4.04$ percent, and reached a maximum value of $w_{ni_{max}} = 41$ centimeters per second, while the maximum flame speed of a propane–air mixture burning from a tube is only 32 centimeters per second, according to H. Brückner (reference 10). This increase of the flame speed, by 28 percent of the tube value, is attributable to the effect of the burner nozzle and was, to a lesser extent, observed also by H. Mache and A. Hebra (reference 6). While these two authors were not able to obtain nozzle-burning cones with excess air, the present writers, using the same size (10 mm) nozzle were able to obtain very beautiful photographs of burning cones with up to 97 percent air, that is, up to an air proportion $\lambda = 1.01$. From air proportion $\lambda = 1.005$ on, corresponding to 3.5 percent by volume propane in the mixture, the flame tended very much to lift off. On the rich side, measurements were made up to about 7 percent propane. For higher values, the cone was not closed enough in the center for practical evaluation.

A completely analogous course was exhibited by the flame speed related to the outer surface with a maximum value of $w_{na_{max}} = 36.6$ cm/sec. The difference, $w_{ni} - w_{na}$, is much greater on the lean side than on the rich side.

No smooth curve can be plotted through the test points of the flames with sound. The points scatter considerably with no definite trend due to intensity being noticeable. In general, however, the flame speed was

increased and the maximum shifted from a propane concentration of x_P = 4.4 percent to x_P = 5.3 percent.

The highest flame speeds appear with relatively weak intensities (f = 0.03 mm to 0.07 mm); $w_{ni_{max}}$ increases from 41 cm per second to 49 cm per second (equal to about 0.1 watt/cm^2), that is, about 20 percent; $w_{na_{max}}$ rises from 36.6 centimeters per second to 42 centimeters per second, that is, about 15 percent. The displacement of the maximum toward seemingly higher propane concentrations suggests that owing to false air supply (agitation effect of sound) to the burning zone by the sound, a clear correlation to the propane concentration is no longer possible. It would also explain the marked scattering of the test values. The assumption that the highest flame speed with sound appears at 4.4 percent propane mixture would mean that the measurable air quantity conveyed into the burning zone by the ponderomotive effects of the sound, at the given relatively weak sound intensities, increases the "false air" by about 22 percent. Since the amount of false air, that is, the agitating effect of the sound, obviously will become greater with rising intensity, the fact that, with very strong sound intensities, the flame is extinguished and cannot be relit would be partly explained; therefore, in the following, only apparent propane concentration and apparent flame speed will be considered.

The flame-speed measurements show, first of all, an increase in the maximum flame speed and, secondly, a strong agitating effect through the ponderomotive force effects of the sound. With the above assumption that the greatest flame speed always appears at the same propane concentration, the true maximum flame speed would be about 22 percent higher than the apparent maximum flame speed.

2. Effect of Sound on the Shape of the Flame

While the sound vibrations raised the apparent maximal flame speed only about 20 percent, instead of an anticipated much higher percentage, the shape of the burning zone was fundamentally changed. The burning zone of the flame without sound has the conical shape with straight sides and rounded tip typical of a flame burning from a nozzle (fig. 12), and adheres closely to the rim of the 10-millimeter-diameter tube. There is no perceptible change at small sound amplitude (f = 0.01 mm) (about 0.012 watt/cm^2), but, when the sound for constant apparent propane concentration and flow volume through the nozzle is progressively increased, the burning zone suddenly jumps somewhat beyond the burner rim at the same time that the height of the cone becomes shorter, while the generating lines exhibit a discontinuity (figs. 12b and 12c), which, with increasing intensity, moves consistently closer to the burner rim. At the same time, the base diameter of the burning zone gets wider and the height of the flame smaller

(figs. 12d to 12g). After passing through certain transitional stages with fluttering or a diffuse luminous upper part of the flatter zones (figs. 12h to 12k), the burning zone finally assumes a quietly burning steel helmet-like shape (figs. 12(l) to 12(o)), which, however, can degenerate into a very flat cup (fig. 12p). On further increasing the sound intensity, the burning zone begins to flutter severely (fig. 12q), to tear open at different points, and finally goes out altogether. Reignition at this stage was, as previously mentioned, not possible.

As shown in the table preceding figure 12, the sound amplitude at which the several developments occur is closely associated with the propane concentration and the flow volume. At high excess of propane, for example, only the base of the flame zone is fundamentally changed, before the violently flickering flame goes out (fig. 12s). In the figures, 12f, 12g, 12r, and 12s, the flame is not located over a sharp rim, but on a smooth wall. In these cases, the sound issuing through the base (of the flame) is considerably greater and the steel helmet-like shape changes into a spherical cap (fig. 12r). Figure 12r was intentionally exposed for a long time to indicate the course of the afterglow of the outer zone while sound is being applied.

In the following, an attempt is made to explain the origin of the pecular shapes of the flame zone. On the whole, three different effects act collectively; first, the flow field produced by the mass flow rate, then the potential field of the sound, and, thirdly, the ponderomotive effects of the sound (sound radiation pressure and sound blast) which increase with the sound intensity. The flow velocity in the nozzle throat ranged between 40 and 220 centimeters per second during these experiments. The cleanest forms of the burning zone (figs. 12(l) to 12(o)) were obtained, depending on the flow velocity, at diaphragm amplitudes of f = 0.03 to 0.10 millimeters. At a frequency of 5000 cycles per second, these values correspond, according to equation (11a), to sound intensities of 0.136 watts per centimeter^2 to 1.51 watts per centimeter^2 and sound velocities $U = \frac{6}{\sqrt{5}} 2\pi\nu f$ of 253 to 844 centimeters per second. The sound velocities in the nozzle throat are therefore 4 to 6 times as high as the flow velocity.

On assuming that the flow field represents only a small disturbance in the potential field produced by the sound, when the velocity of sound is a multiple of the flow velocity, the flow must adjust itself to the potential field. The burning cone must, therefore, assume a shape near to that which would occur in a stationary potential flow. Intermediate shapes originate when sound velocity and flow velocity are comparable. Since the nonaffected gas jet would be able to stay together relatively well, while the sound velocity decreases sharply with the distance from the nozzle, only the lower part of the burning cone is essentially

affected (figs. 12b and 12c). Onto this reciprocal action between flow and sound fields, the sound blast is superposed, which, at small intensities, obviously plays only a subordinate part, but at high intensities predominates.

For the realization of the quasi-stationary potential flow from the nozzle, the following aerodynamic comparison can be applied. On initiating a sudden motion in a fluid at rest, a potential flow sets in in the first instance in which the fluid particles try to flow around existing corners and curvatures; but the flow soon separates at the obstacles and the so-called "starting vortices" result; so, when a previously stationary flow is cut to pieces rhythmically, such as by a quick-closing slide valve, for instance, the obstacles exhibit a series of starting vortices in similar rhythm. At sufficiently high frequency of the interruptor, the starting vortices follow one another so quickly that they cannot develop or separate, so that, on the whole, a potential flow results. In the present case, the burner nozzle represents the obstacle and the vibrating diaphragm the interrupter.

After this physical interpretation of the origin of the new burning zone shapes, it remains to be proved that the burning zone actually assumes the described shape in potential flow. Since the calculation of such a three-dimensional potential flow presents considerable difficulties, several flow measurements were made on electrical models, which are described below.

3. Comparison of the Flame with Sound with the Potential Flow from a Nozzle

In view of the similar construction of the differential equations for potential flow and electric conduction, the potential flow can be determined by measuring the voltage gradients in an electrolyte whose boundary walls, parts of which serve as electrodes, are patterned after the desired flow field.

The experimental apparatus for measuring the potential field in the electrolyte, which will be described in greater detail in a subsequent report, consisted essentially of a massive frame in which a thick, well-leveled crystal glass pane of 1100- by 500-millimeter^2 area was pivotally mounted. The boundaries of the contours of the desired flow field were copied and cemented on the pane. Corresponding parts served as electrodes, and the chamber was filled with a mixture of tap water and distilled water. In this manner, it succeeded in investigating flat fields (with the glass plate horizontal) as well as axially symmetric fields (with the glass plate tilted). In the latter case, the glass plate was tilted approximately 10°,

and so a wedge-shaped sector of the entire body resulted. Above the glass plate, a carriage which carried an exploring electrode could be moved around on rails and was easily adjustable to each point on the electrolyte surface.

Exactly above the exploring electrode was a movably-guided sting which could be jerked upward by electromagnetic release. The whole apparatus was covered with a drawing board with fastened paper so that points could be marked by the point springing up. All metal parts of the apparatus except those serving as electrodes were grounded.

The electrical circuit for measuring the contours is shown in figure 13. The current of a low-frequency transmitter of approximately 800 cycles per second went partly through the parts e_1 and e_2 of the contour serving as electrodes, and through the electrolyte, and partly through the noninductive potentiometers, R_1, R_3, and R_2. A grounded telephone receiver was hooked up between the exploring electrode, e_3, extending in the electrolyte and the resistance R_3. (Note: This was a bridge circuit for setting up a given fraction of the voltage drop on variable resistors, and finding the same fraction on the electrolyte at zero reading.)

To test the usefulness of this apparatus, and especially to test the wedge arrangement, the potential flow through a shutter in a pipe was investigated in the wedge arrangement and as a "half-body problem" (half of form symmetrical about axis of rotation), and also compared with the level problem. A wooden trough 618 millimeters long and 278 millimeters in diameter, coated with a 0.5-millimeter layer of "vinidur" foil to prevent swelling, served as a half body. A semicircular pane of 3-millimeter thick "pertinax"[1] with 51.5 millimeter diameter orifice was cemented into the middle of the trough. Semicircular panes of aluminum foil on each end of the trough served as electrodes. With this electrode arrangement, the field measurements supplied also the equipotential lines of the flow. For the level and the wedge problems, the principal measurements were enlarged in the ratio 1.73 to 1. In the first case, two pertinax strips 5 millimeters thick and 50 millimeters high, one of which represented the axis of the flow, were stuck on the horizontal glass pane. The wedge setup was achieved by a simple cross strut of pertinax. Transverse foil on the ends of the two parallel strips served as electrodes. The water was 47 millimeters deep. For the wedge problem, the pertinax strip serving as axis was replaced by a thread fastened to the glass pane with shellac, the glass pane was tilted 10°, and the enclosure was filled with water until the thread was reached everywhere by the water. The results are represented in figure 14.

---

[1]Trade name for a type of insulating material.

In figure 14 part a represents the electrodes, parts b and c, the insulating pieces, and straight line d, the axis. The solid lines are the equipotential lines of the orifice flow for the wedge arrangement; the dot–dash lines, those for the half–body arrangement; and the dashed lines, those for the level problem. The equal potential difference to the right and left of the orifice section between the electrodes and the exploring electrode was from time to time checked at the potentiometers. At the left hand, these steps, starting from orifice section as zero, were recorded for the two rotationally symmetrical arrangements; on the right hand, for the level problem. The lines for wedge and half–body are fairly close together, except for minor differences, so that only one curve was drawn at many points. Measurements repeated several times disclosed no differences. Following these preparatory tests, the flow in a geometrically similar model of the flame chamber nozzle was investigated. The principal dimensions of the contour are shown in figure 15. The axis was again represented by a thread. A quadrantal arc of a circle of six times the diameter of the nozzle served as electrode at the open side of the nozzle. Herewith, it is assumed that, at this distance from the nozzle throat, the equipotential lines are almost circular. This assumption is well justified, since, at the plane parallel flow from a slot in a flat wall (a case which is easily handled mathematically), the maximum and minimum diameters of the equipotential lines at 5 and 7 slot–width distance from the slot end differ only by 1.6 percent and 0.72 percent from each other.

Figure 16 represents the measured potential field for this nozzle model, each line showing the recorded potential step. As effected in figure 17 for two cases, the exactly measured burning zone in this potential field of the enlarged flame photographs was transcribed on sound–affected flame at the flat wall (heavy curves). At several points of the burning zone, and at right angles to it, the solid arrow indicates the flame speed w_n with opposite sense of direction. From the tips of the flow velocities represented by dashed arrows, a perpendicular was dropped in flame speed direction. According to claims made in section III, 2, the foot of the perpendicular should exactly coincide with the tip of the flame speed arrow.. In view of the previously described secondary effects of other disturbances contained in the chamber while photographing, as well as the inevitable minor drawing mistakes, the agreement as regards the direction and amount of the speeds in several cases is startling. Thus, it is proved that the burning zone, under specified conditions, assumes the sound velocity and the average flow velocity according to a potential flow.

The arrow denoting the speed in figure 17 is obtained as follows: The streamline section between each two potential curves is practically rectilinear in the area under consideration. The difference of the potential steps between each two potential lines divided by the length of this piece of the streamline gives a measure for the flow velocity between

the two potential lines. Their direction is indicated by the assumedly rectilinear piece of streamline. The points, which are not in the exact center between two potential lines, give the speed by interpolation. On the axis, where flow and flame velocity are opposite, an optional value w_n to which all other arrows are referred, was assumed.

Translated by:
Lily Levine
Robert S. Levine
North American Aviation Corporation
and
J. Vanier
National Advisory Committee for Aeronautics

REFERENCES

1. König, R.: Pogg. Ann. Bd. 146, 1872, p. 161.

2. Zickendraht, H.: Über schallempfindliche Flammen, Helv. Phys. Acta. Bd. 14, 1941, pp. 195–214.

3. Damköhler, G.: Der Einfluss der Turbulenz auf die Flammengeschwindigkeit in Gasgenischen. Jahrbuch 1939 der deutschen Luftfahrtforschung, pp. II 3 – II 21. (Available as NACA TM 1112.)

4. Mache, H.: Der Übergang zwischen laminarer und turbulenter Strömung von Gasen in einem kreiszylindrischen Rohr. Forschung Ing.-Wes., Bd. 14, 1943, pp. 77–81.

5. van. de Poll, A. N. J., and Westerdijk, T.: Schlierenaufnahmen von Gasflammen. Zeitschrift für Technische Physik, Bd. 22, 1941, pp. 29–32.

6. Mache, H., and Hebra, A.: Zur Messung der Verbrennungsgeschwindigkeit explosiver Gasgemische. Akad. Wiss. Wien, Math.-naturwiss. Kl., Sitzungsberichte, Abtlg. IIa, Bd. 150, pp. 157–174, Wien 1941

7. Hübner, H. J., and Kläukens, H.: Berechnung der Intensitätsverteilung im Bilde eines Flammenkegels. Ann. Phys., 5. Folge, Bd. 39, 1941, pp. 33–35.

8. Ehret, L., and Hahnemann, H.: Ein neuer Schall- und Ultraschallgeber zur Erzeugung starker Intensitäten in Gasen. Zeitschrift für Technische Physik, Bd. 23, 1942, pp. 245–266.

9. Hartmann, J.: On the production of acoustic waves by means of an air-jet of a velocity exceeding that of sound. Phil. Mag., Ser. 7, Bd. II, 1931, p. 926; also L. Bergmann: Der Ultraschall, VDI-Verlag, Berlin 1939, 2. Aufl., p. 3.

10. Brückner, H., Gastafeln, R., Oldenbourg, München and Berlin 1937, p. 123.

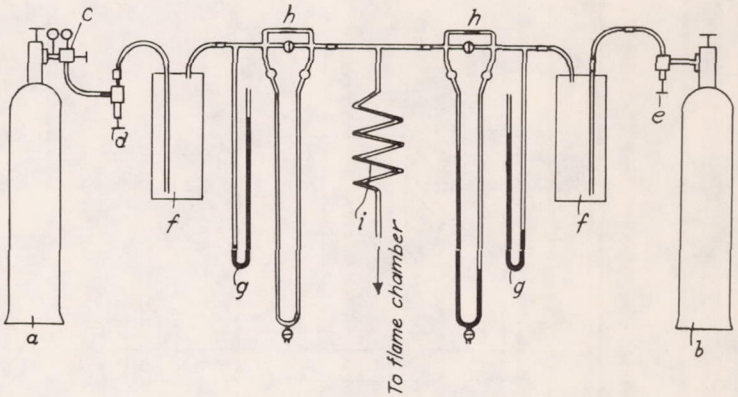

(a) Compressed-air flask
(b) Propane flask
(c) Pressure-relief valve
(d,e) Hofer-angle valve
(f) Steadying flasks
(g) Static pressure gage
(h) Flow capillaries
(i) Mixing coil

Figure 1.- Diagrammatic representation of mixing process.

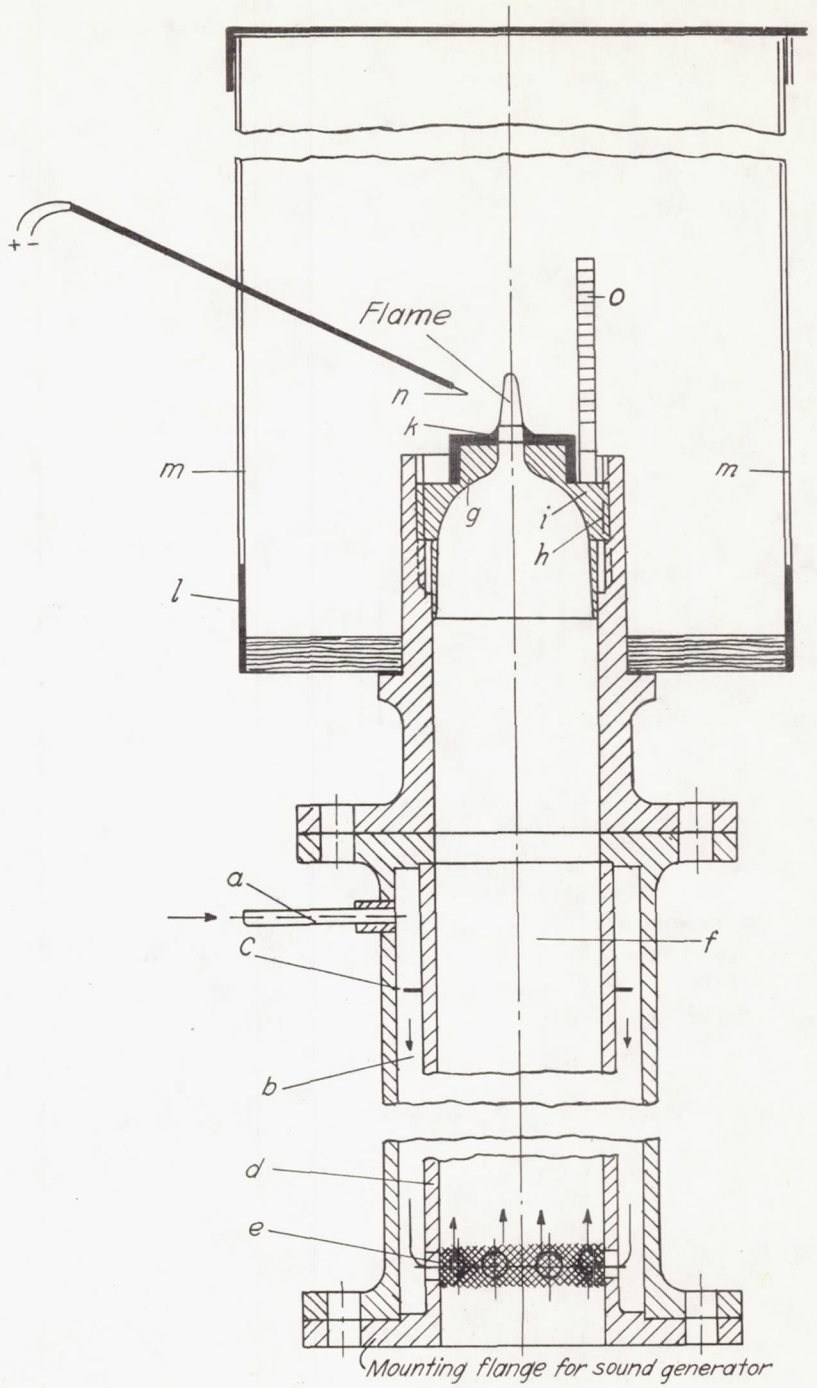

(a) Inlet orifice
(b) Outer cylinder annular chamber
(c) Annular diaphragm
(d) Inner cylinder
(e) Wire screens
(f) Inner-cylinder chamber
(g) Burning nozzle
(h) Threads for nozzle height adjustment
(i) Nozzle body for heat removal
(k) Cylindrical hole with sharp rim
(l) Protective case
(m) Observation window
(n) Hot-wire ignition
(o) Scale

Figure 2.- Flame chamber.

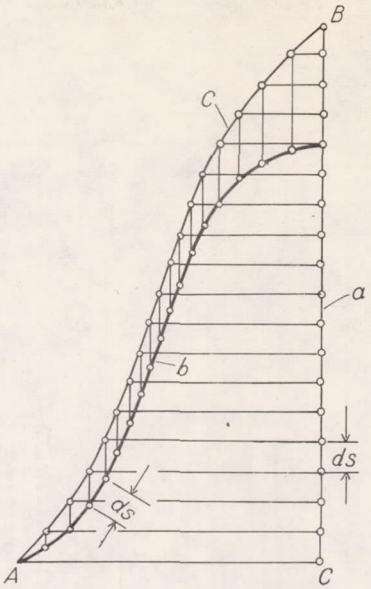

(a) Axis of flame cone
(b) Contour line of flame cone
(ds) Length element

(c) Surface curve
2π x area ABC = surface of flame cone

Figure 3.- Explanation of flame surface.

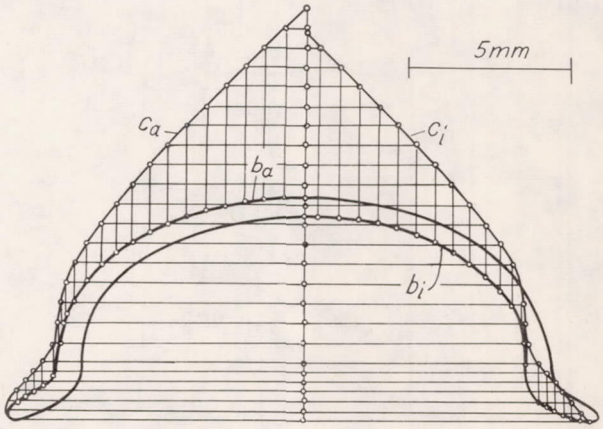

Nozzle diameter 10 mm
Normal volume of mixture 79.0 cm^3/sec
Composition: propane, 5.3 percent by volume
air, 94.7 percent by volume
Amplitude of vibration f = 0.031 mm and frequency ν = 4840 cps of sound

b_a outer burning surface c_a = curves relating to b_a
b_i inner burning surface c_i = curves relating to b_i
} for planimetering (cf. curve c, fig. 3)

Inner flame surface $F_i = 3.49$ cm^2
Maximum flame speed $w_{ni} = 22.6$ cm/sec
Outer flame surface $F_a = 3.98$ cm^2
Minimum flame speed $w_{na} = 19.8$ cm/sec

Figure 4.- Specimen flame surface determination of a flame with slight sound vibrations.

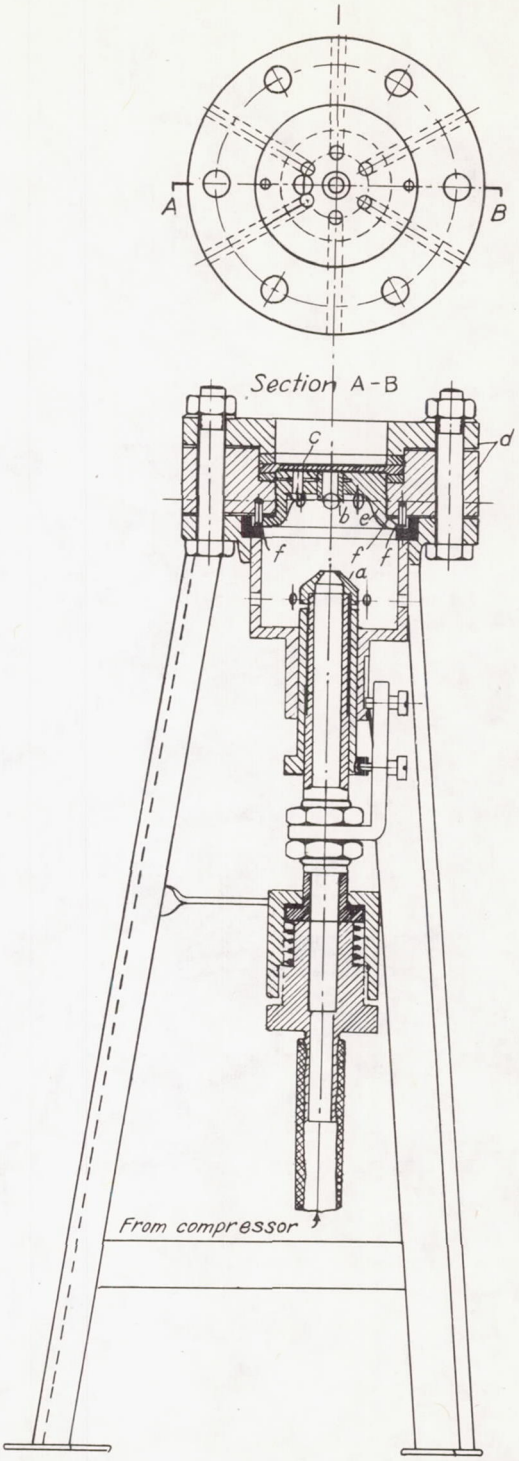

(a) Compressed-air nozzle
(b) Resonator
(c) Beaded diaphragm of electron
(d) Clamping body for diaphragm, also mounting flange for flame chamber
(e) Resonator holder, electrically insulated
(f) Electrical insulation

Figure 5.- The aerodynamic plate vibrator.

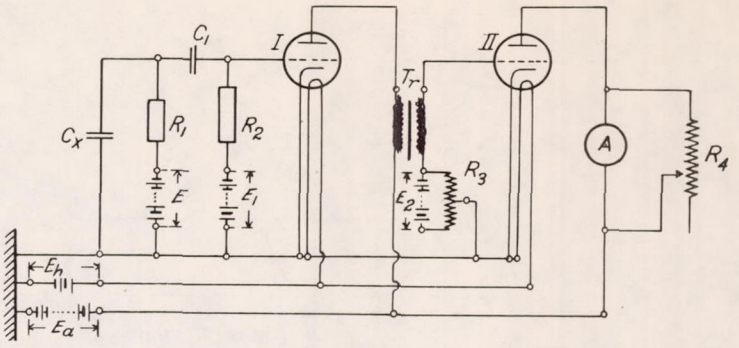

C_x Condenser built up from diaphragm c and resonator holder e (fig. 5)
C_1 Blocking condenser of 0.01 microfarad
R_1 Ohmic resistance, 90 megohms
R_2 Grid resistance, 10 megohms
R_3 Potentiometer, 10 kilohms
R_4 Resistor for controlling sensitivity of ammeter A
I and II Radio tubes (Telefunken) Type AC_2
Tr Transformer
E_h Filament voltage for tubes I and II
E_a Plate voltage for tubes I and II
E D-c. voltage for condenser C_x
E_1, E_2 Grid voltage for tubes I and II

Figure 6.- Wiring diagram of amplitude meter (instrument A).

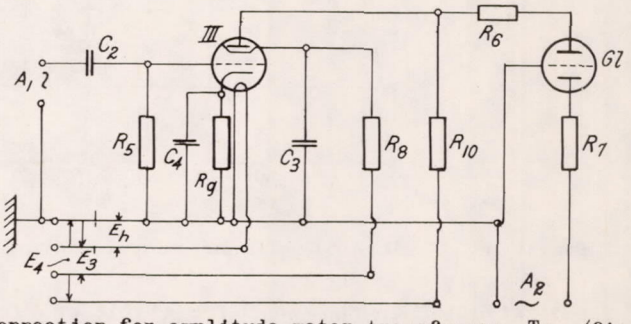

A_1 Connection for amplitude meter transformer Tr (fig. 6)
A_2 Connection for calibrated buzzer
C_2 Bridge condenser, 0.02 microfarad
C_3 Blocking condenser, 1.0 microfarad
C_4 Blocking condenser, 300 microfarads
R_5 Grid resistance, 0.5 megohm
R_6 Output control resistance, 20 kilohms
R_7 Output control resistance, 20 kilohms
R_8 Screen grid leak, 200 kilohms
R_9 Cathode grid leak, 1 kilohm
R_{10} Output control resistance, 50 kilohms
E_h Filament voltage
E_3 Shielded grid voltage
E_4 Plate voltage
Gl Glow-discharge lamp

Figure 7.- Electric hookup for frequency measurement.

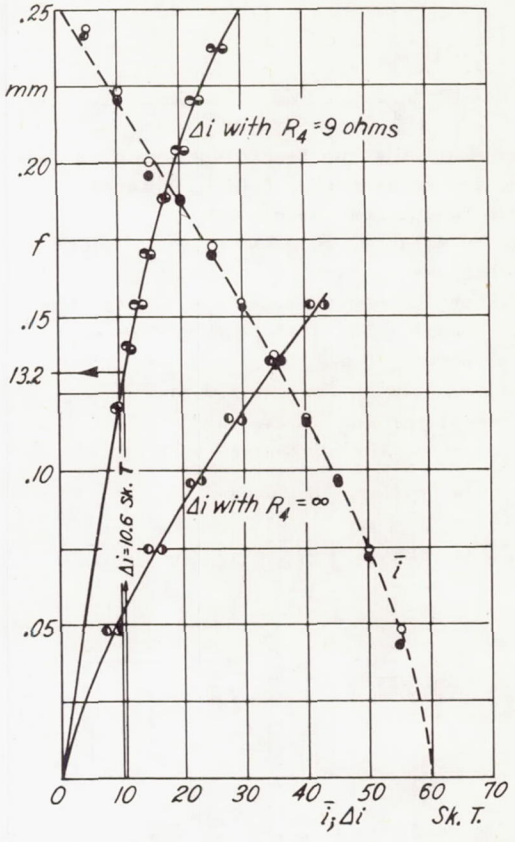

f = amplitude of vibrating diaphragm and distance of dial gage lever from static diaphragm

$\bar{i}$ = indication of instrument B for static or vibrating diaphragm (scale divisions)

Δi = difference in instrument A readings for static and vibrating diaphragm

R_4 = test range resistance

Figure 8.- Explanation of diaphragm vibration amplitude setup.

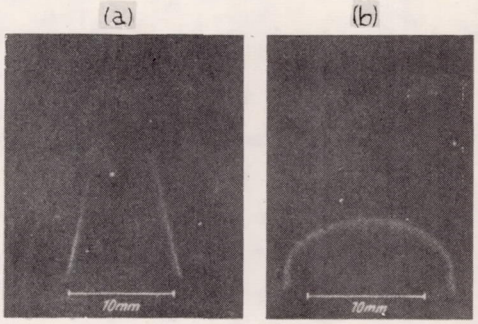

Figure 9.- Burning zone of flame without sound (a), and with sound (b) for the example of table 1.

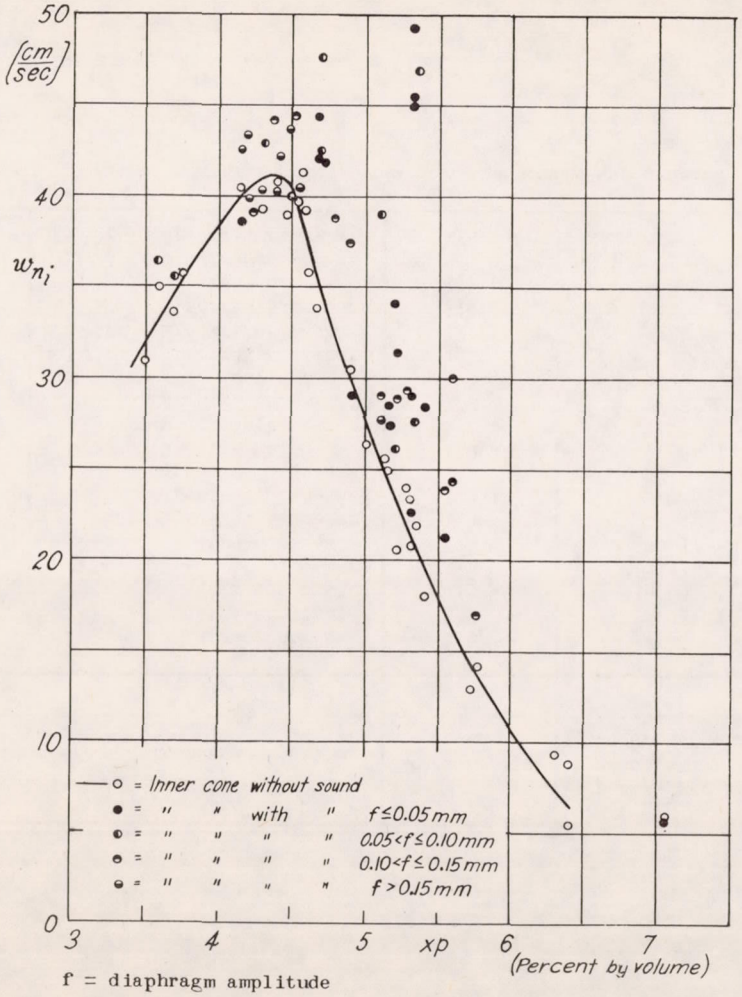

Figure 10.- Inner flame speed w_{ni} plotted against propane concentration x_p without sound and with sound.

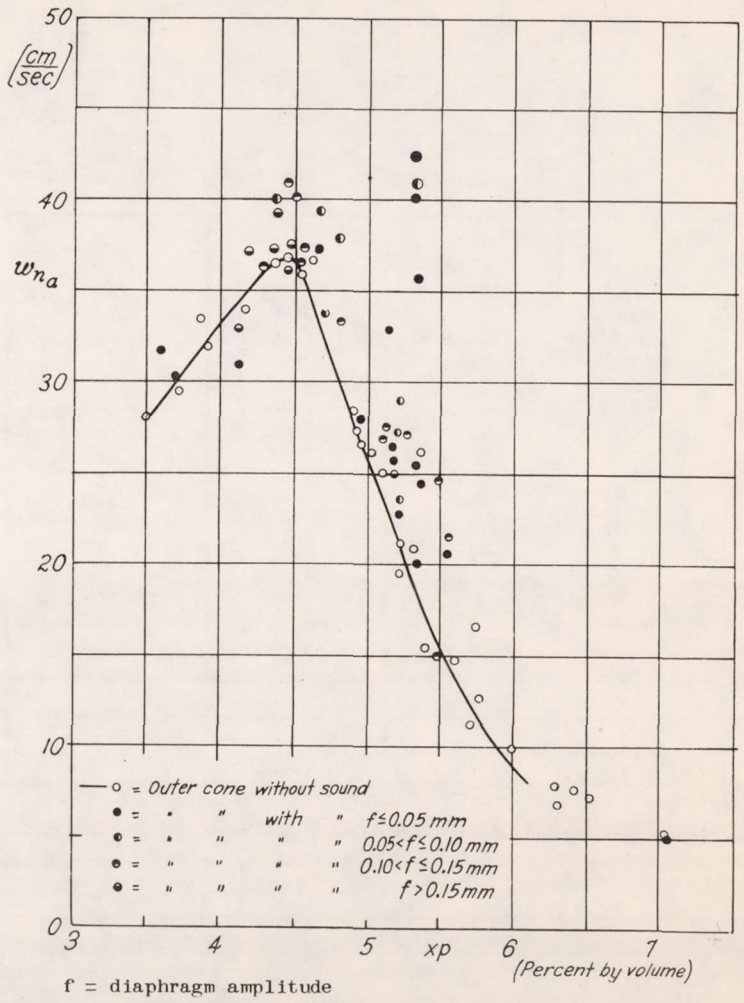

Figure 11.- Outer flame speed w_{na} plotted against propane concentration x_p with and without sound.

TABLE FOR FIGURE 12

No. of photograph	No. of exposure	Type of plate	Exposure time (sec)	Apparent propane concentration x_P in percent by volume	Measured normal volume $V_{nL} + V_{nP}$ cm^3/sec	Flame speed on the inside w_{ni} cm/sec	With or without sound	Diaphragm amplitude f (mm)
a	137	Afga-contrast	1/5	4.46	132	38.5	Without	0.000
b	142	Afga-contrast	1/5	4.63	142	41.7	With	0.03
c	143	Afga-contrast	1/5	4.63	142	42.1	With	0.05
d	120	Spectral blue-hard	1/4	5.37	88	28.2	With	0.02
e	144	Afga-contrast	1/5	4.63	142	47.7	With	0.07
f*	24	Spectral blue-hard	1/4	5.6	79	----	With	----
g*	38	Spectral blue-hard	1/4	5.6	109	----	With	----
h	110	Spectral blue-hard	1	5.32	95	45	With	0.035
i	109	Spectral blue-hard	1/2	5.32	95	49.2	With	0.04
k	117	Spectral blue-hard	1/2	5.15	122	39.2	With	0.03
l	112	Spectral blue-hard	1/2	5.32	102	29.1	With	0.03
m	100	Isopan F	1/5	5.32	79	22.6	With	0.03
n	105	Spectral blue-hard	1/10	5.21	91	29.0	With	0.056
o	127	Spectral blue-hard	1/10	4.34	89	43.1	With	0.07
p	123	Spectral blue-hard	1/10	4.15	70	38.0	With	0.04
q	138	Afga-contrast	1/5	4.5	147	44.1	With	0.15
r*	5	Isopan-ISS	5	5.5	36.5	----	With	----
s*	32	Spectral blue-hard	1/4	6.9	89	----	With	----

*For these photographs the cylindrical cover on the nozzle was omitted, so that the nozzle discharged in a flat wall.

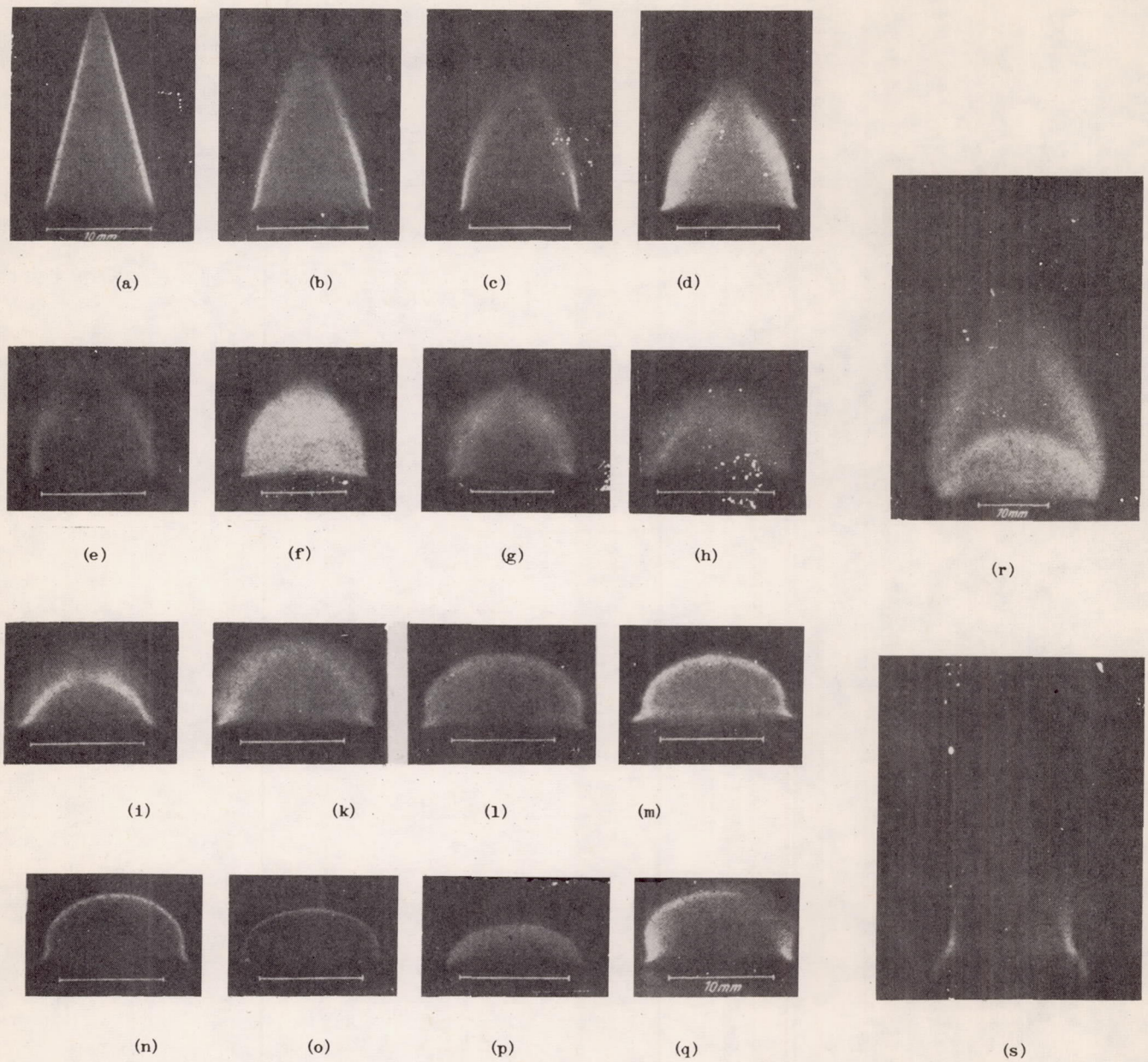

Figure 12.- Effect of sound on shape of burning zone.

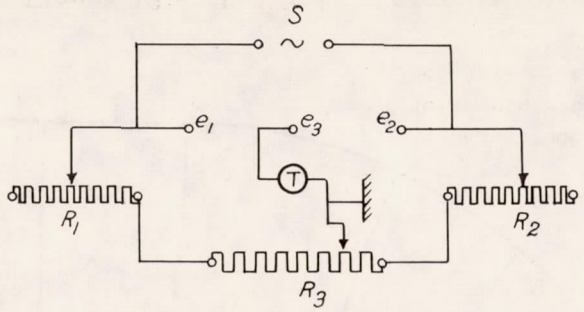

S Low-frequency transmitter, 800 cps
e_1, e_2 Parts of contour serving as electrodes
e_3 Exploring electrode
R_1, R_2 Noninductive lever rheostat with 10 stages of 1000 ohms each
R_3 Noninductive lever rheostat with 10 stages of 100 ohms each
T Telephone receiver

Figure 13.- Electric circuit for measuring the field in the electrolyte.

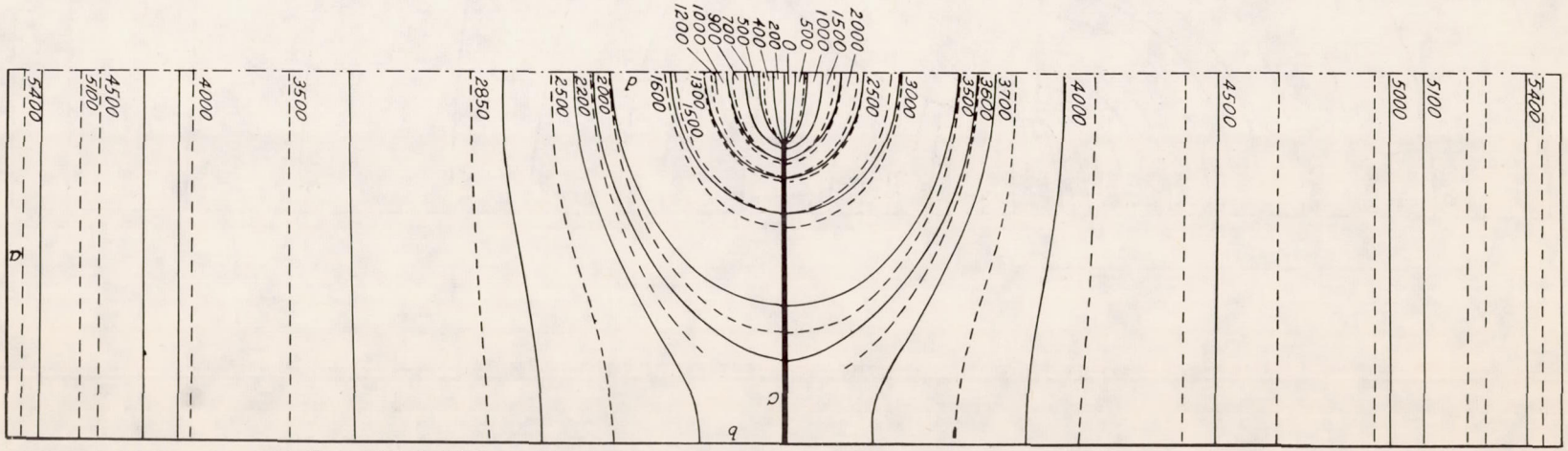

Figure 14.- Comparison of equipotential lines of a diaphragm flow in level wedge-shaped or half-body arrangement.

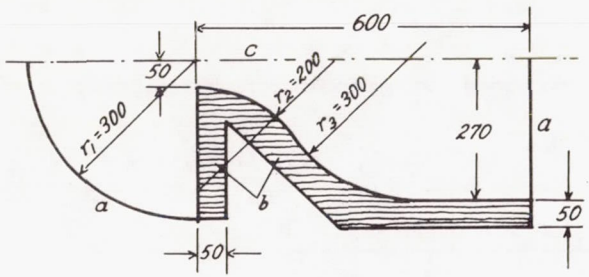

(a) Electrodes
(b) Hard-rubber insulators of contour
(c) Axis of thread

Figure 15.- Principal dimensions of contours of flame chamber nozzle.

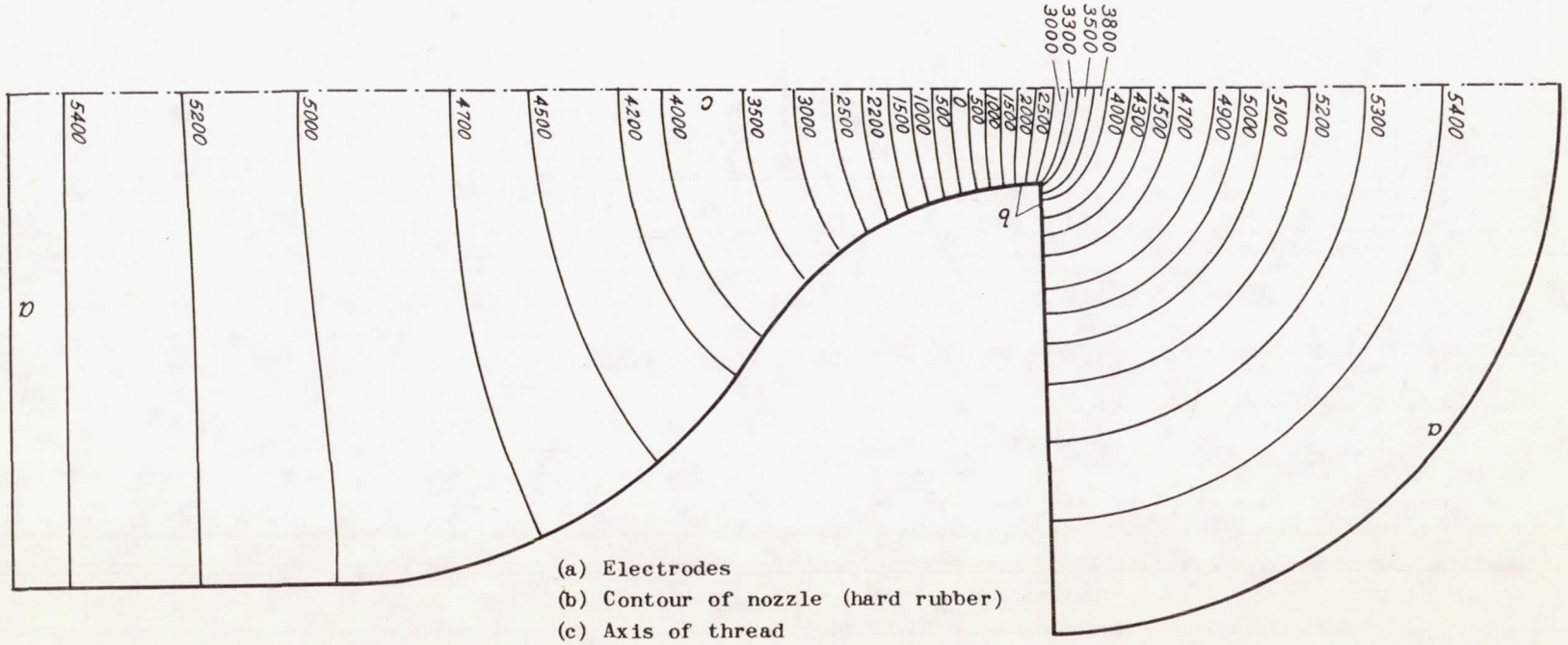

(a) Electrodes
(b) Contour of nozzle (hard rubber)
(c) Axis of thread

Figure 16.- The field of potential lines in the model of the flame chamber nozzle.

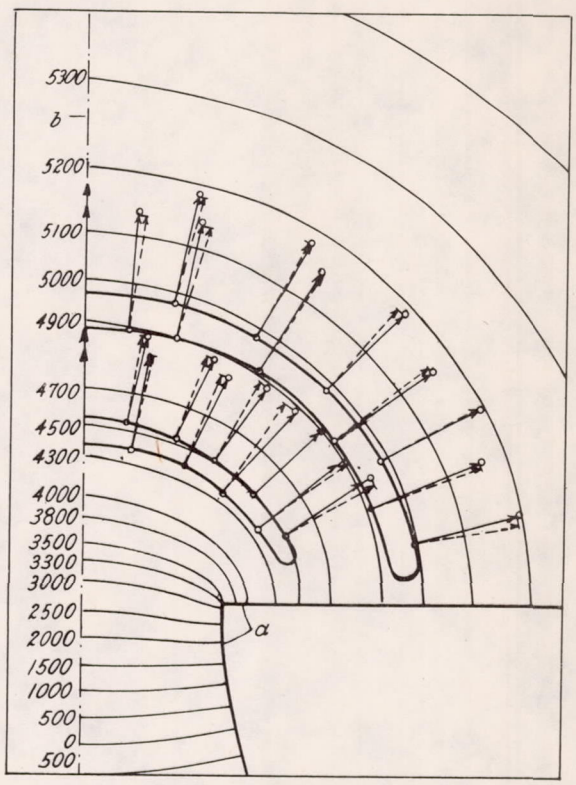

Figure 17.- Comparison of burning zone of flame with sound with potential flow.